Influence of Niobium Pentoxide particulates on the properties of Brushite/Gelatin/Alginate membranes

Influence of niobium pentoxide particulates on the properties of nano-brushite/gelatin/alginate membranes

Hanan H. Beherei[1*], Abdallah A. Shaltout[2,3], Mostafa Mobrouk[1*], Nayera A.M. Abdelwahed[4], Diganta B. Das[5*]

[1]Refractories, Ceramics and Building Materials Department, National Research Centre, 33El Bohouth Street (former EL Tahrir Street.), Dokki, PO Box 12622, Giza, Egypt

[2]Physics Department, Faculty of Science, Taif University, 21974 Taif, P.O. Box 888, Saudi Arabia

[3] Spectroscopy Department, Physics Division, National Research Centre, El Behooth Street, 12622 Dokki, Cairo, Egypt

[4] Chemistry of Natural and Microbial Products Department , Pharmaceutical Industries Division, National Research Centre, 33 EL Bohouth Street (former EL Tahrir Street), Dokki, PO Box 12622, Giza, Egypt

[5] Department of Chemical Engineering, Loughborough University, Loughborough LE113TU, Leicestershire, UK

Submitted for consideration and publication in:

Journal of Pharmaceutical Sciences

21 August 2017

Abstract

Novel non-porous membranes were prepared by impregnating of nano-brushite and niobium pentoxide (Nb_2O_5) into a gelatin/alginate matrix. The physicochemical properties, morphology and mechanical properties of the prepared membranes were characterized using XRD, FTIR, SEM, TEM and universal testing machine, respectively. Swelling ability of the prepared membranes was determined in distilled water. The surfaces of the membranes were characterized by means of FTIR and SEM coupled with EDX after submersion in simulated body fluid (SBF) up to 15 days. Moreover, the calcium and phosphorus ion concentrations in the SBF were measured by UV-spectrophotometer. The *in vitro* drug release and the release mechanism of a model antibiotic, namely, ciprofloxacin (CFX), were tested in phosphate buffer saline (PBS) for 15 days. The antibacterial activities of the CFX-loaded membranes were tested against known microorganisms. The physicochemical properties, morphology, mechanical properties and swelling ability of the prepared membranes were found to be dependent on the presence of Nb_2O_5 allowing control of their properties. For example, the Nb_2O_5-loaded membranes exhibited a higher *in vitro* bioactivity and slower drug release compared to those of Nb_2O_5-free membranes. The CFX-loaded membranes also exhibited an excellent inhibition zones against the selected microorganisms. Overall, the prepared membranes have been found to be very promising for use in bone substitute's applications.

Keywords: Niobium Pentoxide (Nb_2O_5) Particulates; Nano-brushite; Gelatine/Alginate Membranes; Drug delivery.

1. Introduction

Guided tissue regeneration (GTR) is process in which a tissue defect is repaired or new tissue is reconstructed utilizing a barrier membrane (non-porous polymer matrix),which protects the defect site from the overrun/invasion of other tissue, especially fibrous connective tissue[1]. In its original form, GTR technique was established to be an operative procedure in periodontal therapy[2,3,4,5]. The safeguard offered by the membrane maintains the mesenchymal stem cells (MSCs) while allowing cell migration without any obstacles from the embracing periodontium. This enables a construction of new periodontal tissue, particularly precursor bone and periodontal ligament[6]. Two types of implant materials have been reported, namely, resorbable and non-resorbable materials. The resorbable material is

replaced by the host tissue, and typically used as space filling implant. Non-resorbable materials are typically used as structural-support implant[7,8].

The barrier membrane technique is generally utilized to guide bone regeneration in the bone defect site and the term of ’guided bone regeneration (GBR)’has been coined[9,10]. In the past twenty years, resorbable membranes have been investigated and introduced to GTR or GBR techniques. In recent years, resorbable membranes using materials such as chitosan[11], collagen[12] and gelatin/alginate[13] have gained a lot of attention in biomedical applications. However, these membranes possess some drawbacks due to their minimalmechanical strength and lake of physical stability. Therefore, incorporation of inorganic filler is needed to attain improved physico-chemical and mechanical properties for the resorbable membranes while GBR is applied.

With a view to finding optimal alternatives, various composite scaffolds and granules with multifunctional systems have been developed in previous studies[14, 15, 16, 17]. Following the same idea, studies to develop resorbable GBR gelatine/alginate membranes has not been also reported.

Herein we aim to develop gelatin/alginate resorbable membranes (non-porous membrane) through *in situ* incorporation of nano-brushite as well as niobium pentoxide (Nb_2O_5) powder in order to enhance their bioactivity and biodegradation. Nano-brushite is selected due to its impressive properties including biocompatibility, biodegradation and fast disillusion rate which are all very favorable for *in vitro* and *in vivo* biomineralization in the tissue[18]. Nb_2O_5 system has shown certain promise as a nominee material for bioactive coatings on metallic implants[19,20]. Furthermore, the potential uses of these materials for medical implants are growing due to their impressive features such as high corrosion resistance and thermodynamic stability[20,21]. The osteoblasts preferentially adherence to the nano-sized Nb_2O_5 coatings roughness on polished CP titanium was studied by Eisenbarth et al.[22] Accordingly, Nb_2O_5particulate was selected to be loaded at different concentrations in gelatin/alginate membranes to improve the biocompatibility of the prepared systems. Moreover, physicochemical properties of the prepared membranes were determined by X-rays diffractometer (XRD) and Fourier-transform infrared spectroscopy(FTIR). The morphology of the prepared membranes was recorded by scanning electron microscopy (SEM) and transmission electron microscopy (TEM). Mechanical properties were measured by a universal testing machine. The experiments for determining swelling ability and *in vitro* biomineralization were conducted in distilled water and SBF, respectively. Finally, the drug delivery and release kinetics were determined in phosphate buffer saline (PBS).The

antibacterial activities of an antibiotic, namely, ciprofloxacin (CFX) loaded membranes were also tested.

2. Materials and experimental methods

2.1. Materials

Gelatin from calf bone (Gel, medical grade, 280–320 bloom, type A), barium chloride ($BaCl_2$-$2H_2O$) and low viscosity sodium alginate rich in a-L-guluronic residues (approximately 70% of G-block content) were obtained from Sigma-Aldrich, Germany. Niobium pentaoxide (99.5%) was purchased from SPEX Industrial Inc., USA. The simulated body fluid (SBF) and phosphate buffer saline (PBS) were procured from Sigma-Aldrich. For the drug release studies polyvinylpyrrolidone (PVP) (molecular weight = 400000 $g.mol^{-1}$) was purchased from Sigma-Aldrich, Germany, and ciprofloxacin (CFX) (molecular weight 331.34 g.mol-1 and ≥98.0% (HPLC)) was obtained from Fluka Analytical, Germany. All other chemicals for antimicrobial assay were purchased from Sigma-Aldrich, Germany.

2.2. Preparation of nano-brushite

Nano-brushite powder was synthesized by a chemical precipitation method reported earlier[23], briefly following the procedure as follows. 40.0g of ammonium dihydrogen phosphate ($NH_4H_2PO_4$) was dissolved in distilled water (340mL) at a pH value of 3.9. Thereafter, 10.0g of calcite ($CaCO_3$) powder was added to the above solution at the room temperature (25ºC) and stirred for 30min (500rpm)at a pH 5.9. The precipitates formed at the end of the stirring were collected by filtration and washed with distilled water for several times. Subsequently, the obtained powder was dried in oven at 70ºC to obtain 14.64g of nano-brushite. The particulates in the powder have the water lily morphology[23].

2.3. Preparation of non-porous membranes

The prepared nano-brushite was mixed with different ratios of niobium pentaoxide (Nb_2O_5 99.5%). The mixtures were then loaded onto the polymeric matrix for synthesizing four different membranes as demonstrated in Table 1.

INSERT TABLE 1

The polymeric mixture was prepared by mixing equal ratios of gelatin and sodium alginate and stirred vigorously at 40°C in order to obtain a homogenized solution. Firstly, gelatin solution (20% $^{wt}/_{wt}$) and sodium alginate solution (4%$^{wt}/_{wt}$) were synthesized by dissolving the polysaccharide in distilled water at 40°C. Thereafter, a fixed weight of the filler mixture (3.5g) was blended with the polymer mixture and kept at 40°C in a water bath for 30min. Then, four mixtures of membrane were cast into petri dishes and kept at 4°C. The hardened gels were further crosslinked by immersing in $BaCl_2$ solution for 2h, and the non-reacted $BaCl_2$was eliminated by rinsing. After the cross-linking process, membranes with 10mm diameter and 3mm height were dried for 24h at 50°C. Preparation method of the Nb_2O_5-loaded gelatin/alginate membranes is illustrated at Fig. 1.

INSERT FIGURE 1

2.4. Physicochemical properties of the prepared membranes

2.4.1. Phase analysis

In order to achieve information about the obtained phases for the prepared membranes before and after loading nano-brushite and Nb_2O_5 XRD measurements were conducted. The X-ray diffraction analyses were performed with the help of model D8 FOCUS Bruker, Germany with a θ–θ goniometer (diameter 401mm), equipped with a Cu-tube with excitation conditions of 36mA and 45kV, and a scintillation counter.

2.4.2. Fourier transform infrared (FTIR) spectra of the prepared membranes

FTIR spectra of the fabricated membranes were determined using KBr pellets containing membranes powder (200:2 $^{Wt}/_{Wt}$ ratio). These pellets were scanned from 400 to 4000cm^{-1} using a Nexus 670, Nicloet FTIR spectrometer.

2.5. Particle morphology and size

The particle morphology and size of the prepared nano-brushite were determined using SEM (SEM Model Philips XL 30 with accelerating voltage 30KV, England). Particle sample was mounted on stubs with adhesive carbon tape and sputter-coated by means of gold prior to assessment. Moreover, the particle morphology and size of the fillers within the membrane polymer matrix were recorded using TEM (JEM2010, Japan) operating at 200 kV.

2.6. Mechanical properties

Mechanical characterizations of the prepared membranes before and after Nb_2O_5 loading were studied utilizing a universal testing machine (Zwick Roell- Z0.5 TH Mechanical TestEquipment, Germany) equipped with a 1kN load cell. Membranes specimens of cross sectional area 20mm × 50mmwere tested by utilizing a gauge length of 25mm and a crosshead speed of 2mm/min. Five specimens of each membrane were analyzed for their tensile strength (MPa), percentage elongation at break point (%) and Young's modulus (MPa). The above parameters were calculated by the following equations.

$$TS = {}^{F_{max}}/_{A} \quad (1)$$

$$E(\%) = {}^{L}/_{L_o} \times 100 \quad (2)$$

where F_{max} corresponds to the maximum force (N) at break point, A is the cross-sectional area of the sample (mm^2), L is the final length of the specimen at rupture, and L_o (mm) is the original length of the membranes.

2.7. Swelling behavior of the membranes

The swelling capacity of the prepared membranes was estimated as follows. Rectangular specimens with size of 4×6×20 mm^3 were used for the swelling tests in distilled water at 37°C. After immersion for different periods (3, 6, 9, 12, and 15 days), the specimens were taken away from the distilled water, the water excess was eliminated and weighted. Swelling percentage was estimated by equation (3).

$$\mathrm{Sw}(\%) = \left(\frac{W_f - W_i}{W_i}\right) \times 100 \quad (3)$$

The initial weight of the specimen was recorded as W_i and W_f was the specimen weight after immersion. The experiment was carried out three times and the average value was taken in order to determine the result.

2.8. *In vitro* biomineralization test

2.8.1. Surface characterization

Bioactivity of the synthesized membranes was investigated after 15 days of immersion in SBF using FTIR and SEM coupled with energy dispersive X-ray analysis EDX in order to get better understanding for the membranes surface structures.

2.8.2. Variations of ions concentration in SBF

According to the proposed method of Kokubo et al.[24], the membranes were soaked in SBF at 37°C and pH = 7.4 at different time intervals. The Ca^{2+} and P^{+} ions concentrations in the SBF were determined via UV-spectrophotometer (UV-2401PC, UV–VIS recording spectrophotometer, Shimadzu, Japan) utilizing biochemical kits (TechoDiagnostic, USA) at λ=570nm and at λ=675nm, respectively, after immersion times.

2.9. *In vitro* drug release

One of the most common postoperative patient complications upon implantation of synthetic materials is the secondary infections. Therefore, it is highly recommended to incorporate bioactive molecules such as antibiotics into the implanted materials. Ciprofloxacin (CFX) antibiotic was loaded as a model drug to control infection when the membrane is used for GBR.

The membranes were loaded with CFX by dipping the samples into a 20% $^{w}/_{v}$ PVP solution containing the drug. The quantity of loaded drug was ascertained by measuring the drug concentration before and after the dipping in the PVP solution. The solution was filtered, diluted with PBS, and analyzed by UV spectrophotometry. The *in vitro* CFX release was then studied in PBS at pH 7.4 and temperature of 37ºC as follows. Previously heated 50mL of PBS (at 37ºC) was added to a glass vessels maintained at 37ºC within an incubator. After different time intervals, 5mL of the release medium were withdrawn and the concentration of CFX was determined spectrophotometrically at 277nm using UV-Vis spectroscopy (Lambda 25 UV/Vis Spectrophotometer, PerkinElmer, Waltham, MA, USA).

2.10. Mechanism of ciprofloxacin release

Korsmeyer–Peppas model[25] was used to find out the mechanism of drug release from the investigated membranes:

$$M_t/M_\infty = Kt^n \quad (4)$$

where, M_t/M_∞ is the fraction of drug released at time t, k is the rate constant and n is the release exponent. In case of quasi-Fickian diffusion the value of $n<0.5$, Fickian diffusion=0.5, non-Fickian or anomalus transport n=0.5–1.0 and Case II transportn=1.0.

2.11. Antimicrobial assay

To confirm the efficacy of CFX-loaded membrane, the antibacterial activities of the synthesized membranes were tested using agar diffusion method[26] against *Escherichia coli* Northern Regional Research Laboratory(NRRL) B-210 (Gram negative bacteria), *Bacillus*

subtilis NRRL B-543 and *Staphylococcus aureus* NRRL B-313(Gram positive bacteria) sub-cultured into nutrient agar medium. The antifungal activity of these compounds was also tested against *Candida albicans* NRRL Y-477 using Sabouraud dextrose agar medium as follows. Suspension of 0.5 ml of each of the aforementioned microorganisms was added to sterile nutrient agar media at 45°C and the mixture was transferred to sterile petri dishes and allowed to solidify.

Moreover, the membrane samples were cut into 0.5cm×0.5cm square pieces and placed on the surface of the solidified agar plates. The same method was performed using Sabouraud dextrose agar medium using *Candida albicans* NRRL Y-477. All plates were then incubated at 30°C for 24 hours and observed for antimicrobial activity. The diameters of inhibition zone were measured and compared with that of the standard antibiotics and the values were tabulated. Neomycin (10μg) and nalidixic acid (30μg) were used as standard for antibacterial and antifungal activity, respectively.

3. Results and Discussion

3.1 Physicochemical properties of the prepared membranes

3.1.1. Phase analysis

Fig. 2(a) shows the XRD patterns of the prepared membranes before and after Nb_2O_5 loading. The obtained XRD pattern of the prepared nano-brushite-loaded polymer matrix (N_1) possesses a fully crystalline composition. The diffraction peaks of the crystals are assigned to nano-brushite crystal structure (JCPDS file no. 2- 0085) XRD card at 11.63, 20.93, 29.27, 30, 50, 34, 14, 34.41, 41.52 and 50.17 2Θ. No distinct peak of other phosphate phases was recorded. The intensity of the diffraction peaks indicates that the fillers were well crystallized.

The influence of Nb_2O_5 on the obtained phases was estimated by XRD analysis, XRD patterns of the membranes loaded with different percentages of Nb_2O_5 (N2, N3, N4) were zoomed in the range (of 10 to 12) 2Θ as demonstrated in (Fig. 2(b)). The presence of Nb_2O_5showed no characteristic peaks. However, there was a remarkable decrease in the intensity of the diffraction patterns. Consequently, the full width at half maximum decreased with the presence of Nb_2O_5 in the nano-brushite-loaded membranes, thus indicated the decrease of crystallinity and small particle size of the prepared membranes. The XRD results were consistence with the previously reported results[27,28]. However, no remarkable changes

were observed for the nano-brushite-loaded membranes by increasing the Nb_2O_5.The XRD results revealed that the Nb_2O_5 showed no effect on the crystalline phase of the nano-brushite-loaded membranes, however, small decrease in intensity was observed.

INSERT FIGURE 2

3.1.2. FTIR spectra of the prepared membranes

The FTIR analyses are represented in Fig. 2c.Generally, all the prepared membranes exhibited bands at 873cm^{-1} and 1225cm^{-1} attributed to the HPO_2^{-4} group of nano-brushite. N1 possess clearly the characteristic bands of nano-brushite, thus bands were observed at wavelengths of around 525cm^{-1} and 575cm^{-1}. These bands were assigned to the v_4 bending vibrations of the P-O mode. The band at 985cm^{-1}originates due to the P-O(H) v_1 symmetric stretching vibration of PO_3^{-4}. Also, the band around 1060cm^{-1} was assigned to the v_3 vibration of the PO_3^{-4} group. Another band was observed close to 1134cm^{-1}, which was assigned to the v_6 and v_6 degeneration stretch of HPO_2^{-4} ions in nano-brushite. The four sharp characteristics bands between 870cm^{-1} and 1150cm^{-1} were assigned to the P-O/P-O(H) stretching as previously reported[29,30].

The FTIR spectra revealed that the observed bands were similar with those of nano-brushite. For the Nb_2O_5-loaded membranes, remarkable changes were observed as follows. Disappearance of band at 3412cm^{-1} that was attributed to the OH stretching suggested the formation of Nb-OH group, the exemplary band was observed at 3140cm^{-1} owing to the hydroxyl stretching. Moreover, a wide band was noted at 1637cm^{-1} according to adsorbed water on the Nb_2O_5 surface, also the band at 870cm^{-1} that was assigned to Nb-O stretching and bands at 500 and 950cm^{-1} were assigned to Nb–O–Nb angular vibrations also can be observed. Furthermore, the band at approximately 537cm^{-1} was also detected, this band due to O-O type asymmetrical stretching bonded to the metal (Nb-O) and even at 820-870cm^{-1} assigned to the O-O stretching[31, 32, 33].

Furthermore, different bands were obtained for N_2 and N_3. The stretching bands of internal hydroxyls were observed at 3202cm^{-1} and at 3488cm^{-1}, these bands were also observed in the N_4 membrane. The aforementioned bands were more pronounced in the broad spectra of nano-brushite and Nb_2O_5 into the polymer matrix, compared to those of N1 membrane. A strong band was obtained at 1696cm^{-1} regarding the angular deformation of O-H of H_2O adsorbed or adhered to the surface of N4. FTIR results confirmed the impregnation ofNb_2O_5 into the membrane polymer matrix and in line with earlier reported studies[31,32, 33,34].

3.2. Morphology and Size

The morphology of pure nano-brushite filler was investigated by SEM. As illustrated from Fig. 3(a), the prepared nano-brushite exhibited floral-like nanostructures with diameters ranging from 100 to 244nm. It is worthwhile to note that the symmetrical agglomeration of nano-brushite semi-needles was due to the strong attraction force of the layered structure to the particles, which in turn induced the formation of nano-brushite symmetrical agglomeration morphology. Furthermore, the semi-needles morphology consists of similar petal-like flakes growing radically from the centre. SEM image confirmed the XRD results that indicate smaller grain sizes of nano-brushite filler. These results indicate that the medium reagents for precipitation have a strong effect on the crystal structure of nano-brushite as early reported for phosphate ceramic synthesis[35].

INSERT FIGURE 3

Moreover, to determine the effect of Nb_2O_5 on the dispersion behavior of the nano-brushite filler into the polymer matrix, TEM micrographs were recorded for N2, N3 and N4 as illustrated in Fig. 3(b, c and d). All the micrographs showed crystalline aggregates of nano-brushite within the prepared membranes. The influence of Nb_2O_5 to nano-brushite on the microstructure was obvious, the higher Nb_2O_2 the bigger dispersed particles[35,36]. The prepared fillers exhibited defined small crystalline particles (Fig. 3(b, c)), ranging between 100 and 200nm, while clearly defined large crystalline particles with a broad size ranging from 1 to 2µm were obtained for filler within N4 (Fig. 3(d)).

3.3. Mechanical properties

Controlling and understanding mechanical properties are conclusive needs for guided bone regeneration. To determine the effect of the incorporated Nb_2O_2 into the prepared membranes on the physico-mechanical properties, mechanical performance of the membranes was studied by measuring tensile strength, elongation at break point and Young's modulus[36]. All the prepared membranes showed impressive mechanical properties as illustrated at Fig. 3 (e, f and g). The Nb_2O_5-loaded membranes possessed the maximum mechanical values (74MPa, 6.7% and 1980MPa) for tensile strength, elongation at break and Young's modulus, respectively. These results are attributed to the presence of Nb_2O_5. In addition, the incorporation of the Nb_2O_5 into the polymer matrix showed no significant influence on Young's modulus of the membranes as demonstrated in Fig. 3g. According to the results, it can be confirmed that Nb_2O_5-loaded membranes holds the maximum

mechanical performance compared to the Nb_2O_5-free membranes. It is worthwhile to highlight that enhanced mechanical properties would protect the integrity of the membranes and would enable it to induce bone formation without any physico-mechanical deformations[38,39].

3.4. Swelling behavior of membranes

As illustrated in Fig. 4a, the swelling percentage was found to be dependent on the soaking time in the distilled water. Particularly, the swelling percentage increased with the increase of the soaking time. However, the swelling rate becomes slower after long soaking time due to reaching the saturation state. It is worthwhile to note that the swelling percentage decreased with increased Nb_2O_5 weight %. This result could be due to the possible interaction between OH of the gelatin/alginate polymer matrix with the OH groups of nano-brushite or Nb_2O_5, which decreased the free OH content in the membrane. Therefore, a reduction of the hydrophilic properties for all membranes would be expected. This result confirmed that the Nb_2O_5 had enhanced the membrane stability in distilled water when compared with Nb_2O_5-free membranes. The results indicated that the fabricated membranes are capable of absorbing large amounts of water that would induce a better attachment for the surrounding cells into the membrane matrix[40].

3.5. *In vitro*bio-mineralization test

3.5.1. Surface characterization

FTIR spectra of Nb_2O_5-free and loaded membranes are illustrated in Fig. 4 (b, c, d and e) before and post immersion in SBF for several durations. The prepared membranes before and after soaking in SBF for 9 and 15 days confirmed the formation of carbonated apatite deposition onto the membrane surfaces. Generally, all the prepared membranes exhibited the formation of new bands at 460, 863, 965 and 1094cm^{-1} corresponding to PO_4^{-3} and PO, respectively, and the intensity of these bands increased with increased immersion time similar results were reported by[41,42]. In addition, the intensity of the carbonates bands at 1430 and 1630cm^{-1} attributed to C-O and C=O, respectively, were increased after soaking in SBF. The FTIR results revealed that the Nb_2O_5 presence has a significant effect on the biolayer formation as confirmed by the HA groups onto the membrane surfaces such as phosphate (bending and stretching) and OH groups were slightly increased after immersion in SBF compared to Nb_2O_5-free membranes especially after 9 days.

INSERT FIGURE 4

The SEM images of the prepared membranes before and after immersion as well as EDX of membranes surfaces after immersion in SBF are given in Fig. 5.The surface morphology of the prepared Nb_2O_5-free membrane showed a rough structure with some nano-platelets structure as illustrated at Fig. 5 (a, b, c and d). The nanofillers were observed as agglomerates incorporated within the polymer matrix. However, the microstructure of the membrane N3exhibited close, adhered and impressive interfacial attachment between the matrix and the filler, without observation of any cracks or voids in the interface of the components. Furthermore, the microstructures of the membrane N_4exhibitedexcellent dispersion of the nano-fillers in the matrix and good interfacial bonding between the polymer and the nano-fillers. These results confirmed that the presence of Nb_2O_5 had enhanced the dispersion of the nano-filler into the polymer matrix, which is in the same line with TEM results see (Fig. 2(b, c and d)).

The surface of N1 after immersion in SBF showed remarkable changes due to the biodegradation. In addition, a thin layer of precipitated crystals was observed on the membrane surfaces showed in Fig. 5e. Also, there was some dense bright layer onto the surface, confirming faster apatite nucleation. The EDX result recorded small Ca/P ratio (0.9) as showed in Fig. 5i, which is lower than the deficient hydroxyapatite formation (1.67) for after immersion.

INSERT FIGURE 5

For membrane N_2, Fig. 5f showed the occurrence of rough surface including small and large precipitated particles onto the membrane N_2 surface confirming the formation of apatite layer. Also, EDX analysis proved that the precipitated apatite layer on the membrane N_2 surface (1.45) was enhanced compared to membrane N1 Fig. 5j. The result proved that the existence of Nb_2O_5within the polymer matrix enhanced the degree of calcium phosphate precipitation.

SEM coupled with EDX (Ca/P:1.64) Fig. 5 (g and k) of N3 after immersion in SBF exhibited a rough surface with bright longitudinal nodes proved the bio-deposition of bone like apatite. Also, the existence of concentrated global structure with bright color and some corrosion were observed. Thus, this confirmed the precipitation of bone-like apatite layer. On the other side the SEM coupled with EDX analysis Fig. 5 (h, l) of N4 surface proved that the deposited apatite layer on the membrane (1.67) was enhanced compared to other

membranes, and the Ca/P ratio is typically the same as the hydroxyapatite ratio (Ca/P:1.67)[43]. These results confirmed that the higher Nb_2O_5 into the polymer matrix the higher calcium phosphate precipitations.

3.5.2. Ions concentration in SBF

Fig. 6(a, b and c) depicts the release of Ca^{2+}, P^{+} ions in SBF and the Ca/P ratio up to 15 days for all the prepared membranes. The Nb_2O_5-loaded membranes recorded low values of Ca^{2+} ions concentration in SBF (43.04%±0.50, 41.54±0.56% and 31.39±0.67%) compared to Nb_2O_5-free membranes (44.04%±0.85) as showed in Fig. 6a. These results suggested a higher Ca^{2+} ions deposition on the surfaces of Nb_2O_5-loaded membranes. Similarly, lower values of P^{+} ions concentration were recorded for the Nb_2O_5-loaded membranes (25.90±0.45%, 28.00%±1.2 and 32.25%±0.9) compared to the Nb_2O_5-free membranes (45.50%±01.5) as showed in Fig. 6b. The results suggested that the calcium phosphate layer would be greater on the surface of the Nb_2O_5-loaded membranes as confirmed by SEM coupled with EDX results.

The material with potential bioactivity could be *in vitro* analyzed in SBF, because it is much cheaper and quicker than other *in vitro* methods. It could provide evidences for understanding of the basic principle of interaction between bone and biomaterials[40,41]. The implication of the present results on biolayer formation is predicted through calculating the ratio Ca^{2+}/P^{+} for each immersion period of the membranes with various concentrations as showed in Fig. 6c. It is worthy to highlight that the values of Ca^{2+}/P^{+} ratio higher than 1.6, indicated the precipitation of crystalline apatite structure on the surface of biomaterial according to our previous work[43].

INSERT FIGURE 6

3.6. *In vitro* drug release

To study the influence of Nb_2O_5 loading on the CFX release attitude, *in vitro* drug release studies were carried out for all CFX-loaded membranes in PBS as shown in Fig. 6d. Generally, all the membranes released 15% of CFX after 24h, afterwards, the release behavior followed linear pattern up to 360h. CFX release from both Nb_2O_5-loaded and Nb_2O_5-free membranes was comparatively similar except that the final linear phase from the Nb_2O_5-containing membranes was slightly decreased (5%) and the presence of Nb_2O_5 clearly down-regulated the CFX release rates.

These results were based on the fact that CFX was incorporated into the gelatin/alginate polymer matrix through physical dipping into PVP solution that contains CFX as early mentioned in the methodology section. Therefore the CFX was superficially adsorbed onto the Nb_2O_5-free membranes matrices. The moment that bared to PBS solution the physical bond between CFX and the gelatin/alginate polymer matrix was easily detached due to the hydrophilicity of both PVP and CFX, leading to a significant initial release phase followed by linear behavior up to 360h. In contrast, the presence of Nb_2O_5 formed hydrogen bonding with CFX which relatively decreased the final linear phase of CFX from the Nb_2O_5-loaded membranes. These results were in the line with earlier reported results for sustained drug release from multi-phase blend scaffolds[41,44]. In summary, the higher quantities of Nb_2O_5 regulated the release profiles of CFX from the membranes.

3.7. Mechanism of ciprofloxacin release

The *in vitro* kinetic release of CFX followed diffusion kinetics with r (correlation coefficient) above 0.98[45]. The *in vitro* kinetic release parameters are summarized in Table 2. The CFX release behavior was slower in the case of all Nb_2O_5-loaded membranes when compared to Nb_2O_5-free membranes. However, a small quantity of CFX was released at first from the membranes after little time, at which point the release behavior was found to be constant, thus the obtained curves remained plateau until the end of the study. The Nb_2O_5-loaded membranes were capable to absorb more free-CFX compared to the Nb_2O_5-free membranes, but no impulse release of the antibiotic was observed while the presence of Nb_2O_5 relatively controlled the CFX release. Thus, we can conclude that the CFX released is comparatively controlled by the Nb_2O_5 percentage.

INSERT TABLE 2

3.8. Antimicrobial assay

The inhibition zones of CFX-loaded membranes against the Gram positive bacteria (Bacillus subtilis and Staphylococcus aureus), Gram negative bacteria (Escherichia coli) and Fungi (Candida albicans) were measured using the disc diffusion method according as early reported by Mabrouk et al. [46].All CFX-loaded membranes exhibited great activity against the selected microorganisms. These results were only observed for the CFX-loaded membranes. The CFX-free membranes did not show any antibacterial activity against the same under investigated microorganisms as demonstrated in Fig. 6 (e, f, g and h). This result confirmed the antibacterial activity of the CFX antibiotic as previously reported [42].

INSERT TABLE 3

Conclusions

Multifunctional membranes were fabricated in order to guarantee better physico-chemical-mechanical properties, bioactivity and drug delivery through incorporation of Nb_2O_5as well as nano-brushite. Swelling ability of the membranes was better controlled due to the presence ofNb_2O_5,which in turn provides better stability control in the physiological media (SBF). The *in vitro* biomineralization confirmed that the presence of Nb_2O_5 within polymer matrix had led to a remarkable enhancement on the formation of the apatite layer. It was found that the Ca/P ratio (1.5–1.6) was very close to that of the bone HA (1.67). Moreover, the drug delivering ability of prepared systems also confirmed and the in vitro release behavior followed the first order kinetic mechanism. Furthermore, The CFX antibacterial activity was confirmed for the CFX loaded membranes against the selected microorganisms. Finally, novel membranes with unique bioactivity, mechanical properties, drug delivering ability and antibacterial activity are highly recommended to be applied in bone regeneration as GBR.

Future aspects

The prepared membranes will be tested against normal osteoblast cells to get more data in order to clarify the relationship between the membrane and cells (e.g., osteoinductivity, osteoblast differentiation markers RunX2, osteocalcin, ALP activity).

References

1. Dahlin C, Sennerby L, Lekholm U, Linde A, Nyman S.1989. Generation of new bone around titanium implants using a membrane technique: An experimental study in rabbits, Int. J. Oral Maxillofac. Implants. 4: 19–25.
2. Moses O, Pitaru S, Artzi Z, Nemcovsky CE.2005. Healing of dehiscence-type defects in implants placed together with different barrier membranes: A comparative clinical study, Clin. Oral Implants Res. 16: 210–219.
3. Lee J-Y, Lee J, Kim Y-K. 2013. Comparative analysis of guided bone regeneration using autogenous tooth bone graft material with and without resorbable membrane, J. Dent. Sci. 8: 281–286.

4. Beitlitum I, Artzi Z, CE. 2010. Nemcovsky, Clinical evaluation of particulate allogeneic with and without autogenous bone grafts and resorbable collagen membranes for bone augmentation of atrophic alveolar ridges: Bone augmentation with allo- and autografts and collagen membrane, Clin. Oral Implants Res. 2: 1242–1250.
5. Retzepi M, Donos N. 2010. Guided bone regeneration: Biological principle and therapeutic applications. Clin. Oral Implants Res. 21 (2010) 567–576.
6. Dimitriou R, Mataliotakis GI, Calori GM, Giannoudis PV. 2012. The role of barrier membranes for guided bone regeneration and restoration of large bone defects: Current experimental and clinical evidence, BMC Med. 10: 1–24.
7. Sowmya S, Bumgardener JD, Chennazhi KP, Nair SV, Jayakumar R. 2013. Role of nanostructured biopolymers and bioceramics in enamel, dentin and periodontal tissue regeneration, Prog. Polym. Sci. 38: 1748–1772.
8. Braddock M, Houston P, Campbell C, Ashcroft P. 2001. Born Again Bone: Tissue Engineering for Bone Repair, News Physiol. Sci. 16: 208–213.
9. Cai Y, Guo J, Chen C, Yao C, Chung S-M, Yao J, Lee I-S, Kong X. 2017. Silk fibroin membrane used for guided bone tissue regeneration, Materials Science and Engineering C 70: 148–154.
10. Malmström J, Anderudl J, Abrahamsson P, Wälivaara D-À, Isaksson SG, Adolfsson E. 2016. Guided bone regeneration using individualized ceramic sheets, Int. J. Oral Maxillofac. Surg. 45: 1246–1252.
11. Lee B-S, Lee C-C, Lin H-P, Shih W-A, Hsieh W-L, Lai C-H, Takeuchi Y, Chen Y-W. 2016. A functional chitosan membrane with grafted epigallocatechin-3-gallate and lovastatin enhances periodontal tissue regeneration in dogs, Carbohydrate Polymers 151: 790–802.
12. Hadzik J, Kubasiewicz-Ross P, Kunert-Keil C, Jurczyszyn K, Nawrot-Hadzik I, M. Dominiak, Gedrange T. 2016. A silver carp skin derived collagen in bone defect treatment-Ahistological study in a rat model, Annals of Anatomy 208: 123–128.
13. Graulus G-J, Mignon A, Vlierberghe SV, Declercq H, Fehér K, Cornelissen M, Martins JC, Dubruel P. 2015. Cross-linkable alginate-graft-gelatin copolymers for tissue engineering applications, European Polymer Journal 72: 494–506.
14. Sharma C, Dinda AK, Potdar PD, Chou C-F, Mishra NC. 2016. Fabrication and characterization of novel nano-biocomposite scaffold of chitosan–gelatin–alginate–hydroxyapatite for bone tissue engineering, Materials Science and Engineering C. 64: 416–427.

15. Sarker A, Amirian J, Min YK, Lee BT. 2015. HAp granules encapsulated oxidized alginate–gelatin–biphasiccalcium phosphate hydrogel for bone regeneration. International Journal of Biological Macromolecules 81: 898–911.
16. Dong Z, Wang Q, Du Y. 2006. Alginate/gelatin blend films and their properties for drug controlled release, Journal of Membrane Science 280: 37–44.
17. Li Y, Jia H, Cheng Q, Pan F, Jiang Z. 2011. Sodium alginate–gelatin polyelectrolyte complex membranes with both high water vapor permeance and high permselectivity, Journal of Membrane Science 375: 304–312.
18. Kodaka T, Kobori M, Hirayama A, Abe M. 1999. Abrasion of human enamel by brushing with a commercial dentifrice containing hydroxyapatite crystals in vitro, Journal of Electron Microscopy. 48: 167-172.
19. Olivares-Navarrete R, Olaya JJ, Ramírez C, Rodil SE. 2011. Biocompatibility of niobium coatings, Coatings;1 (1): 72–87.
20. Ramírez G, Rodil SE, Muhl S, Turcio-Ortega D, Olaya JJ, Rivera M, Camps E, Escobar-Alarcón L. 2010. Amorphous niobium oxide thin films, J. Non-Cryst. Solids 356 (50–51): 2714–2721.
21. Nascimento WJ, Bonadio TGM, Freitas VF, Weinand WR, Baesso ML, Lima WM. 2011. Nanostructured Nb_2O_5–natural hydroxyapatite formed by the mechanical alloying method: a bulk composite, Mater. Chem. Phys. 130 (1–2): 84–89.
22. Eisenbarth E, et al. 2006. Nanostructured niobium oxide coatings influence osteoblast adhesion, Journal of Biomedical Materials Research Part A. 79A (1): 166–175.
23. Berry EE, & Baddiel CB. 1967. The infra-red spectrum of dicalcium phosphate dihydrate (brushite), Spectrochimica Acta Part A: Molecular Spectroscopy 23: 2089–2097.
24. Kokubo T, Takadama H. 2006. How useful is SBF in predicting in vivo bone bioactivity?, Biomaterials 27: 2907–2915.
25. Korsmeyer RW and Peppas NA. 1983. in: Mansdorf SZ and Roseman TJ (Eds.). Controlled Release Systems, Marcel Dekker, New York, p. 77.
26. Cruickshank R, Duguid JP, Marion BP, Swain RHA. 1975. Medicinal Microbiology, twelfth ed., vol. II, Churchill Livingstone, London, pp. 196-202.
27. Suryanarayana C. 2001. Mechanical alloying and milling, Prog. Mater. Sci. 46: 39.
28. Nascimento WJ, Bonadio TGM, Freitas VF, Weinand WR, Baesso ML, Lima WM. 2011. Nanostructured Nb_2O_5–natural hydroxyapatite formed by the mechanical alloying method: A bulk composite, Materials Chemistry and Physics 130: 84– 89.

29. Pennel G, Leroy G, Rey C, Sombret B, Huvenne JP, Bres E. 1997. Infrared and Raman microspectrometry study of fluoro-fluoro-hydroxy and hydroxy-apatite powders, Journal of Material Science: Materials in Medicine. 8: 271– 276.
30. Wang J, Fu W, Zhang D, Yu X, Li J, Wan C. 2010. Evaluation of novel alginate dialdehyde cross-linked chitosan/calcium polyphosphate composite scaffolds for meniscus tissue engineering, Carbohydrate Polymers 79: 705–710.
31. Prasetyoko D, Ramli Z, Endud S, Nur H. 2005. Preparation and characterization of bifunctional oxidative and acidic catalysts Nb_2O_5/TS-1 for synthesis of diols, Materials Chemistry and Physics 93: 443–449.
32. Marco P and Lorens J. 2007. Understanding of naphthalene sulfonate formaldehyde condensates as a dispersing agent to stabilise raw porcelain gres suspensions: Surface adsorption and rheological behaviour, Colloids & Surfaces A, 299 (1-3): 180-185.
33. Colthup N, Daly L, Wiberley S. 1975. Introduction to infrared and Raman spectroscopy. Academic Press, New York.
34. Goncalves M, Oliveira L, Guerreiro M. 2008. Magnetic niobia as adsorbent of organic contaminants in aqueous medium: effect of temperature and pH, Quim. Nova 31: 518.
35. Pradhan D, Wren AW, Misture ST, Mellott NP. 2016. Investigating the structure and biocompatibility of niobiumand titanium oxides as coatings for orthopedic metallic implants, Materials Science and Engineering C. 58: 918–926.
36. Pauline SA, and Rajendran N. 2014. Biomimetic novel nanoporous niobium oxide coating for orthopaedic applications, Applied Surface Science 290: 448– 457.
37. Cuppoletti J. 2011. Metal, ceramic and polymeric composites for various uses. InS. M. Mousavinasab (Ed.), Effects of filler content on mechanical and optical properties of dental composite resins. Shanghai, China: InTech.
38. Liu X, Wang T, Chow LC, Yang M, Mitchell JW. 2014. Effects of inorganic fillers on the thermal and mechanical properties of poly(lactic acid), International Journal of Polymer Science 2014: 1–8.
39. Rubab Z, Afzal A, Siddiqi HM, Saeed S. 2014. Preparation, characterization :and enhanced thermal and mechanical properties of epoxy-titania composites, The Scientific World Journal 2014: 1–7.
40. Vlierberghe sv, Dubruel P, Schacht E. 2011. Biopolymer-Based Hydrogels As Scaffolds for Tissue Engineering Applications: A Review. Biomacromolecules 12(5): 1387–1408.

41. Mabrouk M, Choonara YE, Kumar P, Toit LC du, Pillay V. 2016. Effect of Lyophilized EmuGel Silica Microspheres on the Physicomechanical Properties, *In Vitro* Bioactivity and Biodegradation of a Novel Ciprofloxacin-Loaded PCL/PAA blend Scaffold, Polymers 8 : 232; doi:10.3390/polym8060232.
42. Mabrouk M, Choonara YE, Marimuthu T, Kumar P, Toit LC du, Vuuren SV, Pillay V. 2016. $Ca_3(PO_4)_2$ Precipitated Layering of an In Situ Hybridized PVA/Ca_2O_4Si NanoFibrous Antibacterial Wound Dressing, International Journal of Pharmaceutics 507: 41–49.
43. Boulila S, Oudadesse H, Badraoui R, Lefeuvre B, Mabrouk M, Chaabouni K, Mostafa A, Makni-Ayedi F, Barroug A, Rebai T, Elfeki A, Elfek H. 2016. Antioxidative/oxidative effects and retarding osteoconductivity of ciprofloxacin-loaded porous polyvinyl alcohol/bioactive glass hybrid. Med Biol Eng Comput. doi 10.1007/s11517-016-1473-1.
44. Mabrouk M, Mulla JAS, Kumar P, Chejara DR, Badhe RV, Choonara YE, Toit LC du, Pillay V. 2015. Intestinal Targeting of Ganciclovir Release Employing a Novel HEC-PAA Blended Lyomatrix, AAPS Pharm Sci Tech, doi: 10.1208/s12249-015-0442-6.
45. Ashfaq M, Khan S, Verma N. 2014. Synthesis of PVA-CAP-based biomaterial in situ dispersed with Cu nanoparticles and carbon micro-nanofibers for antibiotic drug delivery applications, Biochemical Engineering Journal 90: 79–89.
46. Mabrouk M, Selim MM, Beherei H, and El Gohary MI. 2013. Incorporation Effect of silver and zinc-zeolites into commercial Glass Ionomer Cement. Interceram 62 (1): 50-54.

Figures Caption

Fig. 1. Preparation method of the Nb_2O_5-loaded gelatin/alginate membranes.

Fig. 2. Illustrations of a) XRD spectra of N2, N3 and N4 with reference to N1 (5- 60) 2Θ, b) (10-12) 2Θ and c) FTIR spectra of N2 , N3 and N4 with reference to N1.

Fig. 3. Illustration of a) SEM of the nano-brushite; TEM images of b)N2, c)N3 and d) N4 and, mechanical measurements e) tensile strength, f) elongation at break point and g) Young's modulus of the prepared membranes.

Fig. 4. Demonstration of s the swelling (%) in distilled water at pH 7.4 and incubation temperature of 37°C; FTIR spectra of the prepared membranes b) N1, c) N2, d) N3 and e) N4 before and after immersion in SBF for different time intervals.

Fig. 5. SEM images of the developed non-membrane porous surfaces of a) N1, b) N2, c) N3 and d) N4 as prepared; SEM images of e) N1, f) N2, g) N3 and h) N4 coupled with EDX i) N1, j) N2, k) N3 and l) N4 after 15 days of immersion in SBF.

Fig. 6. Illustrations of a) Ca, b) P ions concentration in SBF and the c) Ca/P ratio up to 15 days of immersion; d) cumulative CFX (%) release in PBS up to 360 hours (15 days) using agar diffusion method e) *Staphylococcus aureus*, f) *Candida albicans*, g) *Bacillus subtilis* and h) *Escherichia coli* with reference to Neomycin antibiotic.

Table 1. Formulation template of nano-brushite and Nb_2O_5-loaded membranes based on the filler weight %.

SN	Membrane code	Nano-brushite (% wt/wt)	polymermatrix (% wt/wt)	Nb_2O_5 (% wt/wt)
1	**N1**	20	80	0
2	**N2**	18	80	2
3	**N3**	16	80	4
4	**N4**	12	80	8

Table 2. *In vitro* kinetic release of CFX from and Nb_2O_5- loaded membranes

	R^2-value†			First-order		n	RE $_{0-360h}$‡
Formula code	**Zero-order**	**First-order**	**Korsmeyer-Peppas model**	**t_{50}* (hours)**	**t_{90}** (hours)**		**(%)**
N1	0,958	0,991	0,883	432,926	1528,135	2,187	45,455
N2	0,956	0,989	0,866	490,675	1728,535	2,059	43,176
N3	0,938	0,983	0,855	587,283	2077,505	1,873	37,575
N4	0,952	0,982	0,849	837,639	2974,928	1,562	35,239

* n is The diffusion exponent

*t_{50} is time required for 50% of the drug to be released

**t_{90} is time required for 90% of the drug to be released

‡RE_{0-360h} is the release efficiency of the drug from 0 to 360 hours

†R^2-value is the value for regression co-efficient

Table 3: Average inhibition zones diameters (mm) measured for the synthesized non-porous membranes.

Sample Code	Gram +ve bacteria		Gram –ve bacteria	Fungi
	Bacillus subtilis	*Staphylococcus aureus*	*Escherichia coli*	***Candida albicans***
N1	-ve	-ve	-ve	**-ve**
N2	-ve	-ve	-ve	**-ve**
N3	-ve	-ve	-ve	**-ve**
N4	-ve	-ve	-ve	**-ve**
N1_CFX	25	25	24	**24**
N2_CFX	24	24	23	**23**
N3_CFX	25	26	24	**25**
N4_CFX	**24**	**25**	**23**	**24**

Highly active (+++)= (inhibition zone > 20 mm)

Moderately active (++)=(inhibition zone 15 - 19 mm)

Slightly active (+)= (inhibition zone 10 - 14 mm)

Inactive (-ve) = (inhibition zone < 10 mm)

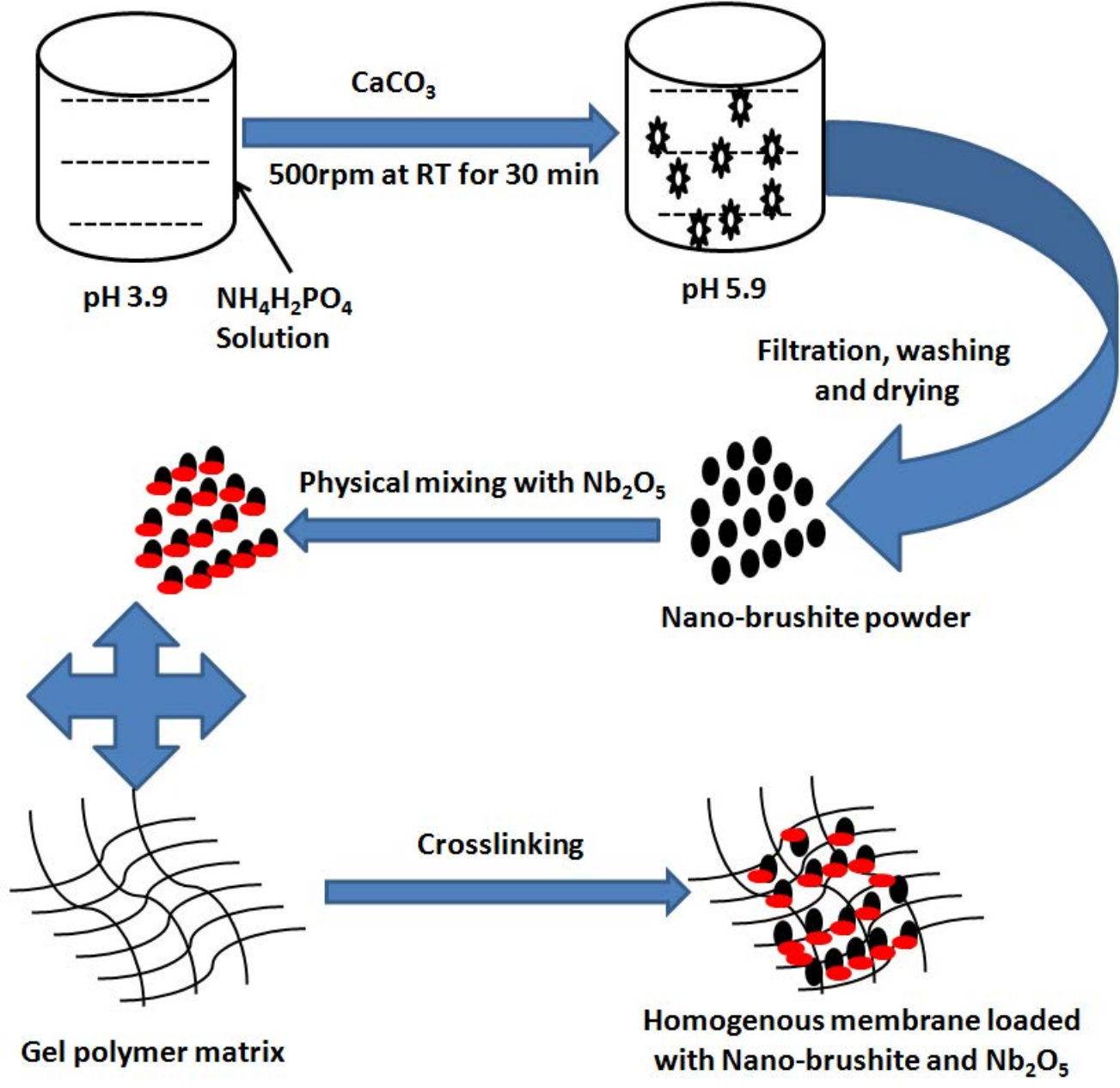
$CaCO_3$
500rpm at RT for 30 min
pH 3.9
$NH_4H_2PO_4$ Solution
pH 5.9
Filtration, washing and drying
Physical mixing with Nb_2O_5
Nano-brushite powder
Crosslinking
Gel polymer matrix
Homogenous membrane loaded with Nano-brushite and Nb_2O_5

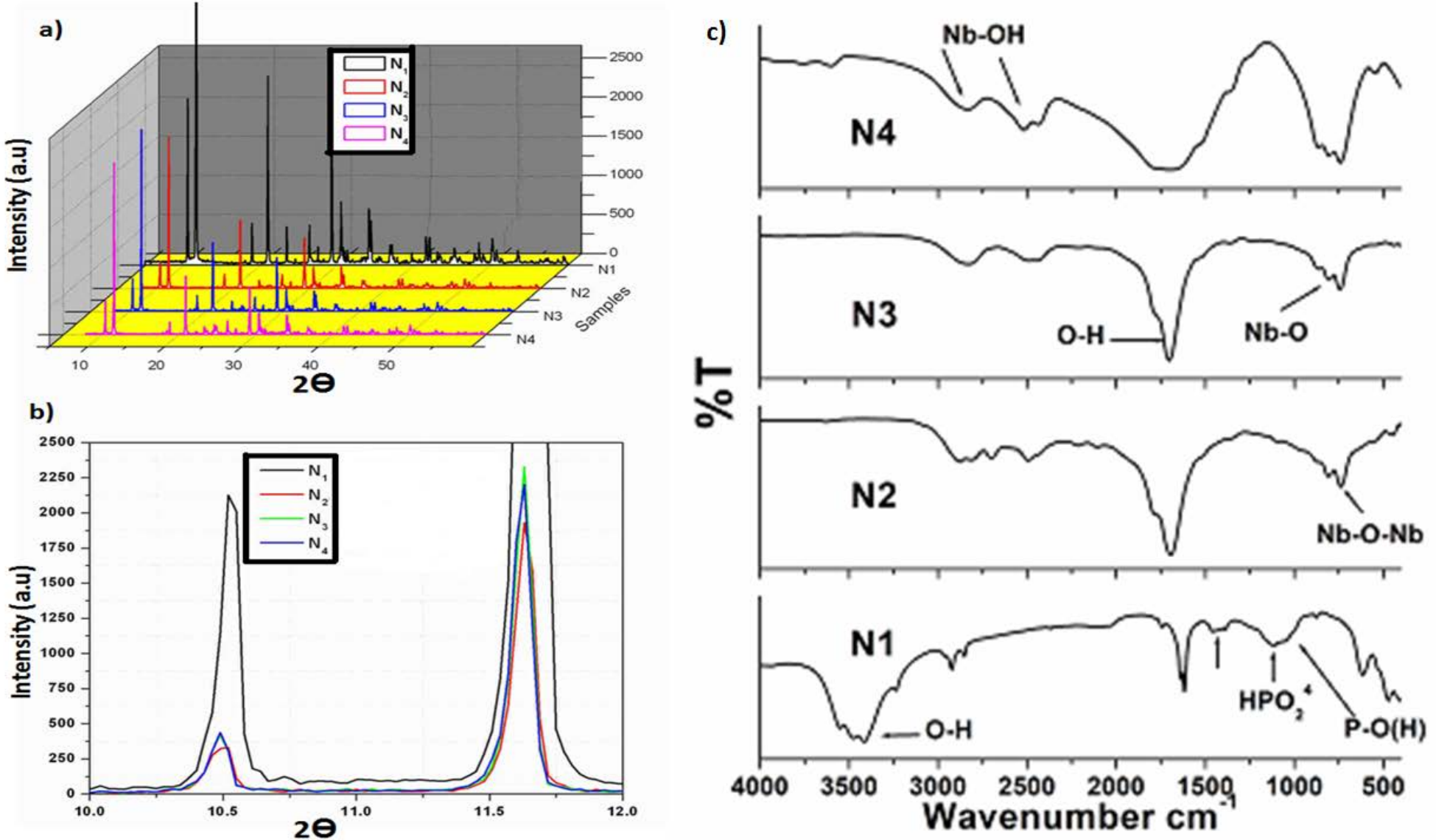
a)
Intensity (a.u)
2Θ
Samples
N1
N2
N3
N4
b)
Intensity (a.u)
2Θ
c)
%T
Nb-OH
N4
N3
O-H
Nb-O
N2
Nb-O-Nb
N1
O-H
HPO4-2
P-O(H)
Wavenumber cm-1

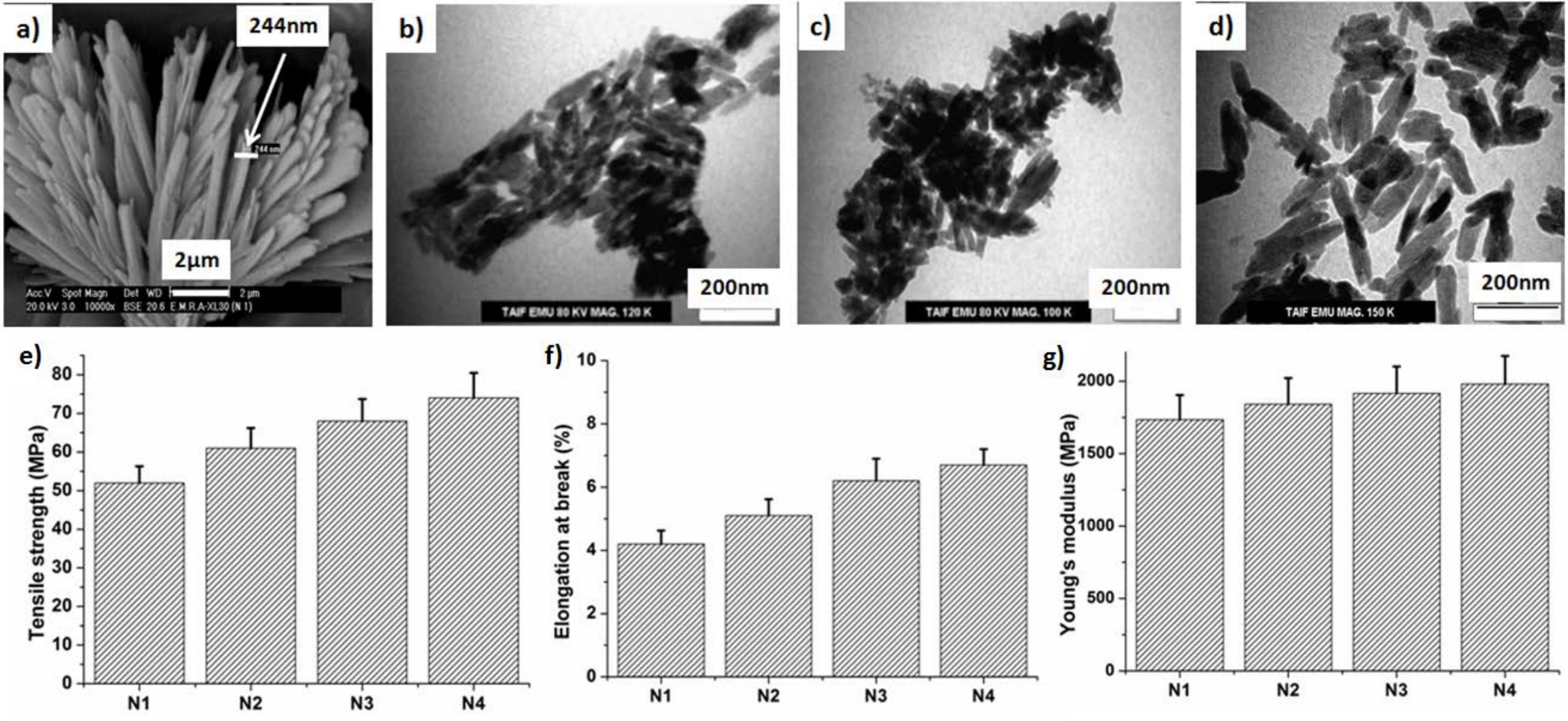
a)
244nm
2µm
b)
200nm
TAIF EMU 80 KV MAG. 120 K
c)
200nm
TAIF EMU 80 KV MAG. 100 K
d)
200nm
TAIF EMU MAG. 150 K
e)
Tensile strength (MPa)
0
10
20
30
40
50
60
70
80
N1
N2
N3
N4
f)
Elongation at break (%)
0
2
4
6
8
10
N1
N2
N3
N4
g)
Young's modulus (MPa)
0
500
1000
1500
2000
N1
N2
N3
N4

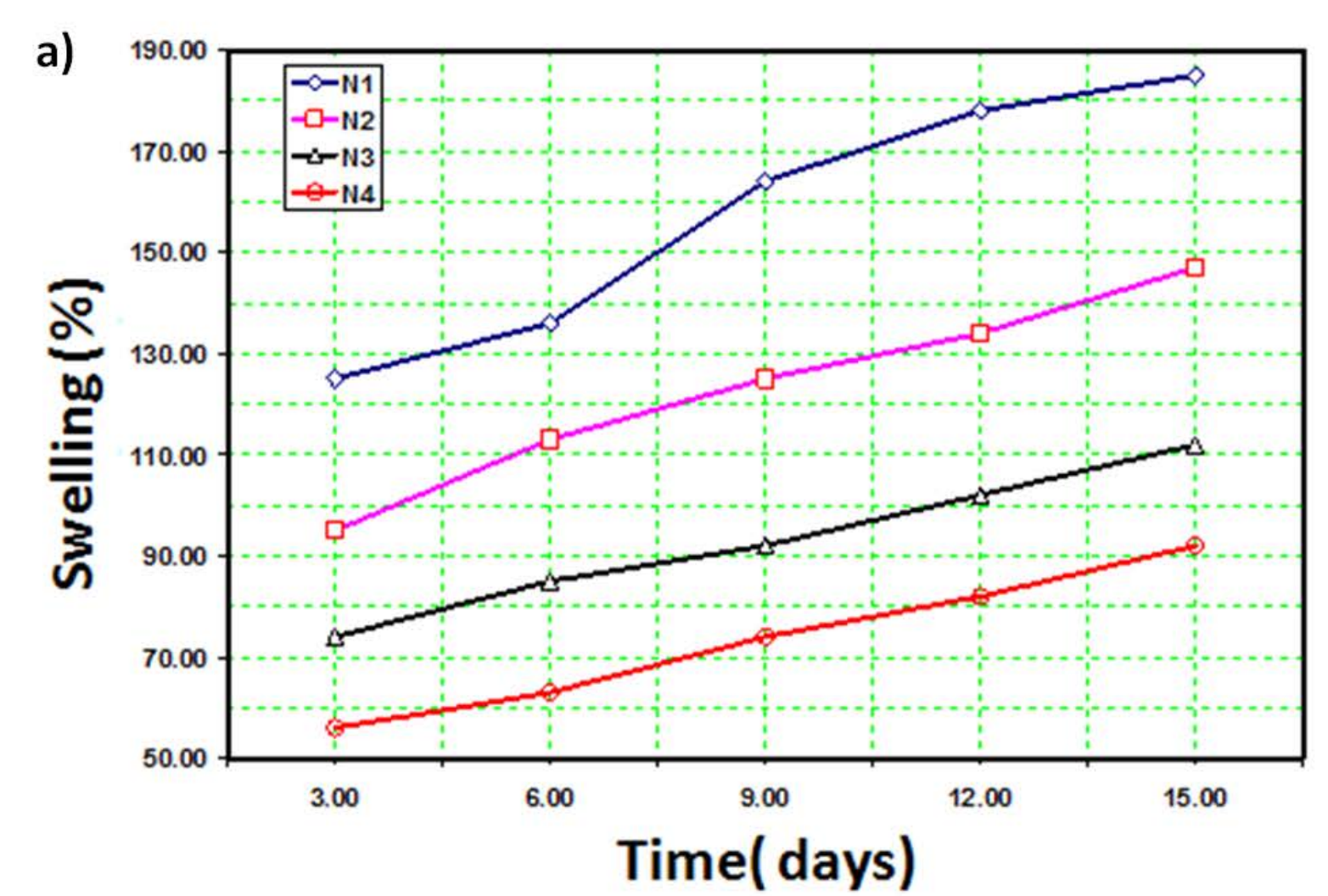
a)
N1
N2
N3
N4
190.00
170.00
150.00
130.00
110.00
90.00
70.00
50.00
Swelling (%)
3.00
6.00
9.00
12.00
15.00
Time(days)

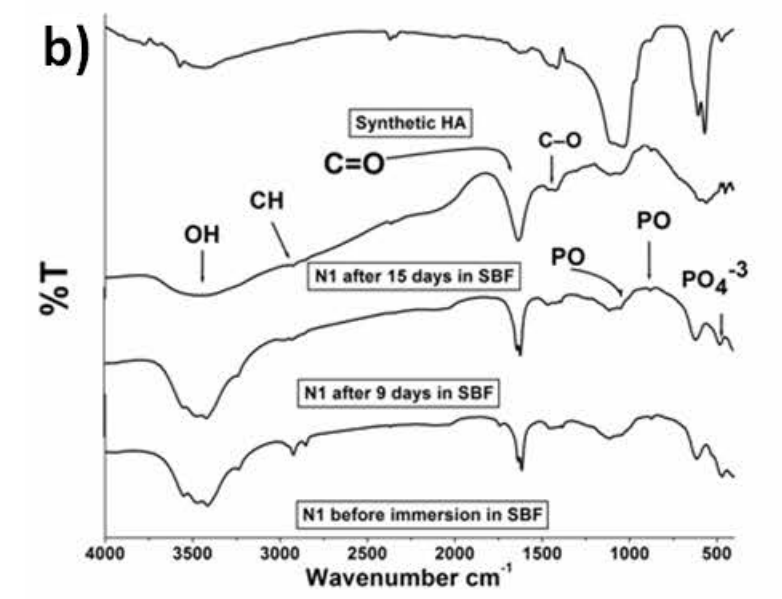
b)
Synthetic HA
C=O
C–O
OH
CH
PO
PO
PO_4^{-3}
N1 after 15 days in SBF
N1 after 9 days in SBF
N1 before immersion in SBF
%T
4000
3500
3000
2500
2000
1500
1000
500
Wavenumber cm^{-1}

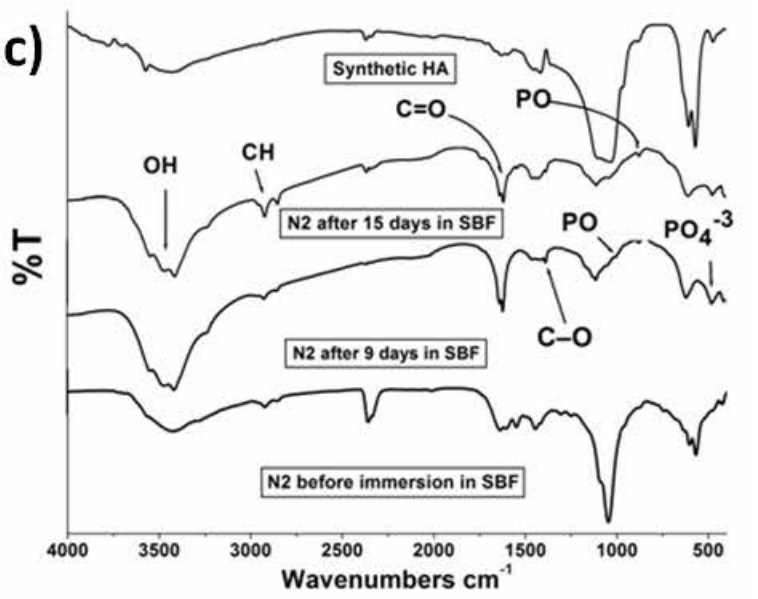
c)
Synthetic HA
C=O
PO
OH
CH
N2 after 15 days in SBF
PO
PO_4^{-3}
C–O
N2 after 9 days in SBF
N2 before immersion in SBF
%T
4000
3500
3000
2500
2000
1500
1000
500
Wavenumbers cm^{-1}

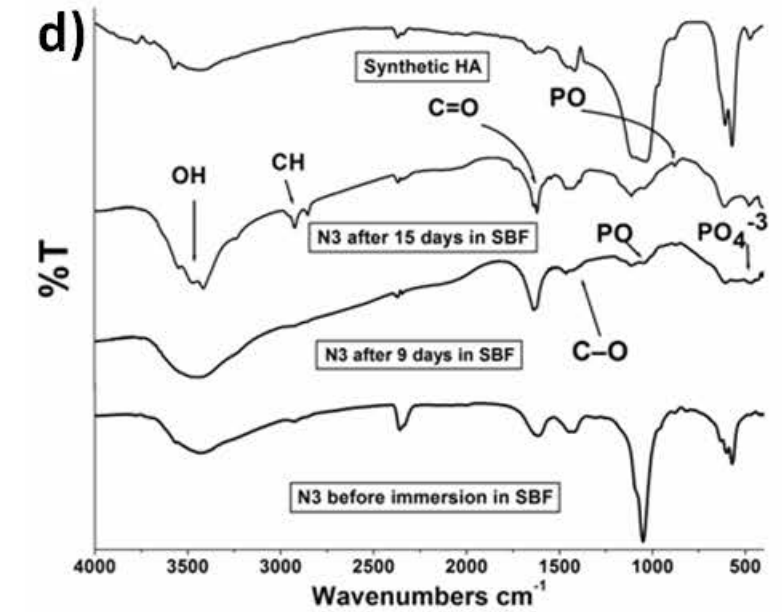
d)
Synthetic HA
C=O
PO
OH
CH
N3 after 15 days in SBF
PO
PO_4^{-3}
C–O
N3 after 9 days in SBF
N3 before immersion in SBF
%T
4000
3500
3000
2500
2000
1500
1000
500
Wavenumbers cm^{-1}

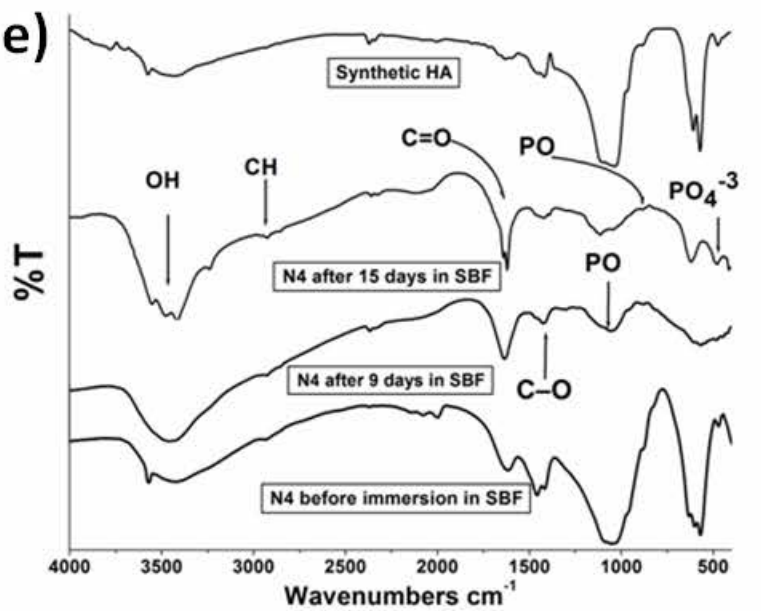
e)
Synthetic HA
C=O
PO
OH
CH
PO
PO_4^{-3}
N4 after 15 days in SBF
PO
C–O
N4 after 9 days in SBF
N4 before immersion in SBF
%T
4000
3500
3000
2500
2000
1500
1000
500
Wavenumbers cm^{-1}

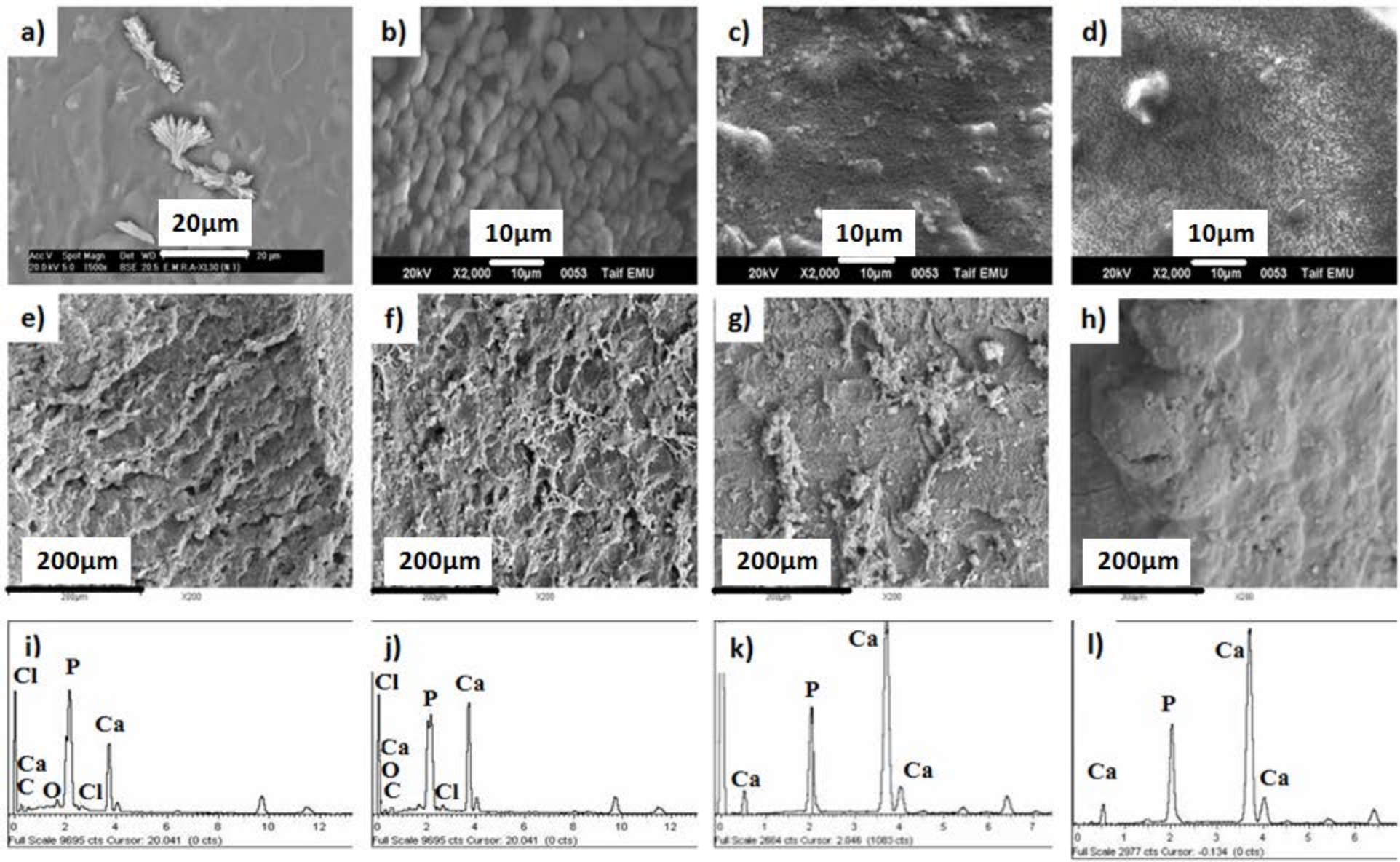
a)
20µm
b)
10µm
20kV X2,000 10µm 0053 Taif EMU
c)
10µm
20kV X2,000 10µm 0053 Taif EMU
d)
10µm
20kV X2,000 10µm 0053 Taif EMU
e)
200µm
f)
200µm
g)
200µm
h)
200µm
i)
Cl
P
Ca
Ca
C
O
Cl
Full Scale 9695 cts Cursor: 20.041 (0 cts)
j)
Cl
P
Ca
Ca
O
C
Cl
Full Scale 9695 cts Cursor: 20.041 (0 cts)
k)
Ca
P
Ca
Ca
Full Scale 2664 cts Cursor: 2.046 (1083 cts)
l)
Ca
P
Ca
Ca
Full Scale 2977 cts Cursor: -0.134 (0 cts)

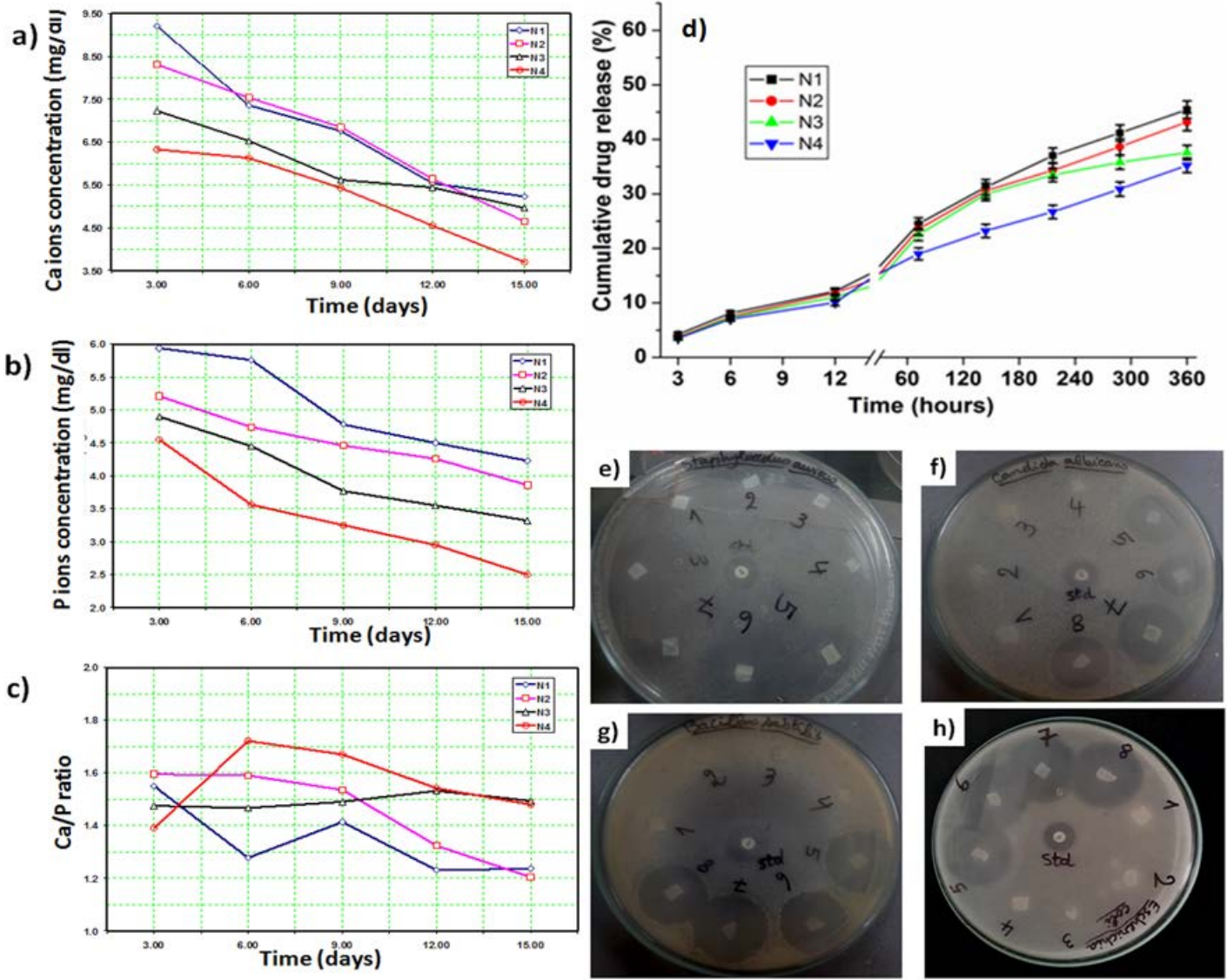
a)
Ca ions concentration (mg/dl)
Time (days)
N1
N2
N3
N4
b)
P ions concentration (mg/dl)
Time (days)
c)
Ca/P ratio
Time (days)
d)
Cumulative drug release (%)
Time (hours)
e)
f)
g)
h)
Std